Protonated Carbon Nitride Incorporated Polyamide Thin Film Nanocomposite for Reverse Osmosis Desalination

A. Abdul Aziz, P. S. Goh*, M. A. Azali, M. N. Zainal Abidin & M. H. Abu Ba'dah

School of Chemical and Energy Engineering, Faculty of Engineering, Universiti Teknologi Malaysia, 81310 UTM Johor Bahru, Johor, Malaysia

ABSTRACT

Protonated carbon nitride (pCN) prepared from acid treatment of carbon nitride (CN) was incorporated in the polysulfone (PSf) substrate and polyamide (PA) layer to produce thin film nanocomposite (TFN) membrane. The hydrophilicity of CN is expected to improve the surface hydrophilicity of the membrane and acid treatment of nanoparticle is aimed to further enhance the surface structure and prevent the agglomeration of nanomaterial from taking place. pCN loading used in the PSf substrate was 0.5% while in the PA layer was varied as 0.05%, 0.1% and 0.15%. All the membrane prepared were characterized in terms of morphology, structural properties, and surface chemistry. Reverse osmosis dead-end filtration system was used to determine the water permeability and the salt rejection. It was observed that, all the membrane prepared could maintain the salt rejection with improvement of water permeability. However, the salt rejection was sacrificed when higher loading of 0.15% pCN was tested, although the water permeability of the membrane has reached approximately 0.5 LMHbar. This work demonstrates that the use of pCN in RO membrane can improve the water permeability without sacrificing the salt rejection.

Keywords: Thin film nanocomposite, carbon nitride, protonated carbon nitride, reverse osmosis, surface modification

1.0 INTRODUCTION

World human populations facing a growth rate of 1.2% per year and is expected to reach up to 14.4 billion peoples in less than 60 years [1]. With the exponential growth of world population, current resources should be taken care of to ensure their sustainability in more generations to come. Fresh water supply is undoubtedly the most vital resource for human life. Source of fresh water should not be taken for granted many parts of the world populations are already lost their supplied for a fresh water. According to United Nations World Water Development Report 2015, there are still 748 million peoples lacking of access to the fresh water supply and the demand for fresh water is estimated to be increased by 400 percent globally by 2050 [2].

Reverse osmosis (RO) is a promising technology in purifying seawater or salt water into a drinking water. It is one of the most reliable techniques to increase the production of fresh water supply among the various existing method. This concept was introduced by Loeb and Sourirajan that included the process of demineralization of the salt water, preparation of the membrane and overall process of RO [3]. In RO process, thin

film composite (TFC) membrane was usually used as a medium to obtain fresh water. TFC membrane comprises of a thin film or polyamide (PA) layer act as a selectivity layer produced from the interfacial polymerization from the reaction between two monomers on top of a porous support membrane [4]. An ideal TFC membranes should possess several key characteristics such as high salt rejection (>98%), high water permeability, excellent mechanical strength and anti-fouling properties.

As a new technology evolved, research on membrane field was also developed to expand their capability and performances. The introduction of nanomaterials is a promising way to address the limitations of TFC membrane such as low water permeability and fouling by introducing the usage of nanofillers in the membrane fabricated either in the support membrane called mixed matrix membrane (MMM) or in a PA layer called thin film nanocomposite (TFN) [5]. By introducing nanomaterials within the membrane, membrane characteristics such as mechanical strength and chemical stability as well as salt separation and water permeability could be greatly improved [6]. In this work, protonated carbon nitride (pCN) was embedded in the support membrane and PA layer, respectively. This intention of the current study was to improve the water permeability performances of the membrane without compromising the salt rejection. Wang *et al.* have evidenced that [7], CN was capable to improve the wettability of the membranes thus improve the hydrophilicity and water permeability. This happen due to the formation of hydrogen bond that present between nitrogen atom of the CN with water molecule. On the other hand, works reported by Wan Azelee *et al.* [8] who

treated their hybrid nanomaterial of multiwalled carbon nanotube and titania nanotube (MWCNT-TNT) with strong acid to positive surface charge have effectively improved the dispersion of nanomaterials in the solutions. Furthermore, the positively charged surface of substrate also positively affected the formation of PA layer, hence resulted in enhanced flux and salt rejection. In this work, pCN was used as nanofillers in the substrate and PA layer to create a positive charge on active layer and thin film so that PA layer would have a stronger attraction within the PSf support layer.

2.0 METHODS

2.1 Materials

Polysulfone Udels P-3500 polymer, supplied in a form of a pellet by Solvay, polyvinylpyrrolidone (PVP, K29-32) and 1-methyl-2-pyrrolidinone (NMP,99.5%) was obtained from Acros Organic were used to develop support membrane. m-Phenylenediamine (MPD,99%) and 1,3,5-benzenetricarbonyl trichloride (TMC,98%) from Acros Organic were used to prepare PA layer (i.e., using PSf as supports). Sodium chloride (NaCl, 99.5%) provided by ACL Labscan and n-hexane (C_6H_6, 49%) were supplied by Merck, while hydrochloric acid (HCl, 65wt%) was obtained from Merck. Melamine was supplied by Sigma-Aldrich.

2.2 Synthesis of Carbon Nitride and Acid Treatment

Melamine was used to fabricate CN through a thermal polycondensation method. In a typical procedure, 10g of

melamine powder was place into a crucible with a lid and then covered the whole crucible with an aluminium foil to prevent from sublimation to happen [9]. Then, the crucible was heated in air condition by a carbolite furnace at 550 °C for 2 h with a heating rate of 5 °C/min. After it was cooled to room temperature, the yellow product was collected and ground into a powder with a ceramic mortar. For pCN, 50 mL of 5 M hydrochloric acid was mixed with 5 grams of CN used. The solution was then stirred overnight, followed by filtration and washing with deionised water until pH become neutral. Lastly, the nanoparticles were dried at 100°C under vacuum.

2.3 Preparation of Polysulfone (PSf) Support Membrane

Phase inversion technique was used to fabricate PSf substrate. The casting solution to produce neat PSf substrates was prepared by dissolving 17.5 wt% PSf in a solvent NMP with 0.5 wt% of PVP. 0.5 wt% of pCN was added in the casting dope solution to prepare PSf substrate that was incorporated with pCN. The dope solution was stirred for 24 h to ensure a good dispersion of pCN. After that, the dope solution was left for sonication in room temperature for 1 to 2 h before proceed to casting to eliminate the air bubbles. The dope solution was then cast onto a clean glass plate using a glass rod and then immersed directly into the coagulation bath containing deionised water. The same procedure was used to prepare neat substrate but without the addition of pCN into the dope solution.

2.4 Preparation of Thin Film Composite and Thin Film Nanocomposite Membranes

PA active layer was prepared by interfacial polymerization method. 2% of MPD in deionised water and 0.1% TMC in n-hexane were used as monomers to form the PA layer on the top of the support membrane. Active layer of the support membrane was placed between a glass plate and the rubber frame and poured the MPD solution. After 1 min, excess MPD solution was drained off and removed the leftover by a rubber roller. Then, TMC solution was dripped on the surface to react with MPD for 50 second. After that, excess TMC solution was poured out and let it dry in ambient temperature for 1 min. The membranes were post-treated in an oven at 60°C for 5min and later stored in DI water for 24 hours before further use.

For TFN membrane, 0.05 w/v%, 0.1 w/v% and 0.15 w/v% of pCN were mixed with the TMC solution. The mixture was then sonicated for 1 h prior to interfacial polymerization to avoid agglomeration of the nanoparticles. The denotations of the TFN membranes prepared in this study are tabulated in Table 1.

Table 1 Denotation use to represent the membranes

Substrate/ support membrane	PA layer	Denotation
17.5 wt% PSf + 0.5 wt% PVP	MPD + TMC	TFC
17.5 wt% PSf + 0.5 wt% PVP + 0.5 wt% pCN	MPD + TMC	pCN-TFN
17.5 wt% PSf + 0.5 wt% PVP + 0.5 wt% pCN	MPD + TMC (0.05 w/v% pCN)	0.05 pCN-pCN-TFN
17.5 wt% PSf + 0.5 wt% PVP + 0.5 wt% pCN	MPD + TMC (0.1 w/v% pCN)	0.1 pCN-pCN-TFN
17.5 wt% PSf + 0.5 wt% PVP + 0.5 wt% pCN	MPD + TMC (0.15 w/v% pCN)	0.15 pCN-pCN-TFN

2.5 Characterization of Nanomaterials and Membranes

Morphology of CN and pCN was analysed by using transmission electron microscopy (TEM, HT 770, Hitachi, Japan). X-ray diffraction (XRD, Cu Kα radiation, λ = 0.154nm, D/max-rB 12 kW Rigaku) was used to examine the crystallinity of the CN and pCN. Other than that, attenuated total reflectance fourier transmission infrared spectroscopy (ATR-FTIR, Thermo Nicolet Avatar 360) was used to identify the functional groups of the nanomaterials and the membranes prepared. To investigate the morphological structure of the membrane, field emission scanning electronic microscope (FESEM, SU8020, Hitachi) was used to have a high-resolution image and energy-dispersive X-ray spectroscopy (EDX) to analyse the element on the samples. Membrane surface charge was determined by zeta potential test (Malvern Zetasizer Nano ZS). Lastly, surface roughness (R_a) was measured by using atomic force microscopy (AFM, SII Nano Technology SPA 300 HV) and the wettability of the membrane was examined using contact angle goniometer (OCA 15 Pro, Dataphysics).

2.6 Evaluation of Membrane Performances

Dead-end filtration system was used to measure RO performance that was made of stainless steel 316 (Model HP4750 Stirred Cell, Sterlitech Corp., Kent, WA). The membrane contact surface area was 14.6 cm^2 (2.26in^2). Firstly, the membrane was stabilized at 16 bar for 30 min with RO water to compact the structure of the membrane and then was reduced to 15 bar for further used. Next, NaCl solution (2000 ppm) was used as feed water and permeated water was collected. The water permeability (*A*) and salt rejection (R) were determined. The water permeability was calculated based the equation:

$$A \text{ (LMHbar)} = \frac{V}{At\Delta P} \qquad (1)$$

where V is volume of permeate water in the experiment, A is the area of membrane, and t is the time of permeate water. While salt rejection was determined by using the equation:

$$R \text{ (\%)} = (1 - Cp/Cf) \; x \; 100 \qquad (2)$$

where C_p is the concentration of permeate solution and C_f is the feed solution concentration.

3.0 RESULT AND DISCUSSIONS

3.1 Characterizations of CN and pCN

Figure 1 shows the morphological structure of CN and pCN obtained from TEM characterization. As can be seen, the morphology of both nanomaterials is with nanosheet graphene-like structure. This observation has been reported by M. Sihor *et al*. [10] and J. Zhu *et al*. [11]. The difference between both nanomaterials was the stacking of nanosheet after the modification using strong acid. The modified CN has created high repulsive forces between the molecular structure by absorbing the positive charge carried by H^+ in HCl thus increase the distance between the sheets. Figure 2 shows the chemical bonding of CN and pCN. The thermal condensation of melamine will

be produced carbon nitride through deamination and formed tri-s-triazine (proved through ATR-FTIR testing on Figure 3). The hydrochloric acid treatment has modified the chemical structure of the carbon nitride by adsorption of hydrogen ion on the nanomaterials surface. This was also stated by Mudunkotuwa *et al*. [12] who modified TiO_2 using adsorption of citric acid with pH range of 2.0, 4.0, 6.0 and 7.5. Higher repulsive forces were experienced by TiO_2 after protonation and increasing of pH solution to acidic could bring the nanomaterials to positively charge. This phenomena can be explained by Derjaguin, Landau, Verwey, and Overbeek theory (DLVO theory) where electrostatic repulsion would increase and the Van Der Waals attraction forces become low when the distances of charged nanosheets increase [13]. By measuring the particles size based on the TEM results, CN possessed an average particle size of 28.96 nm and pCN showed approximately of 37.47 nm
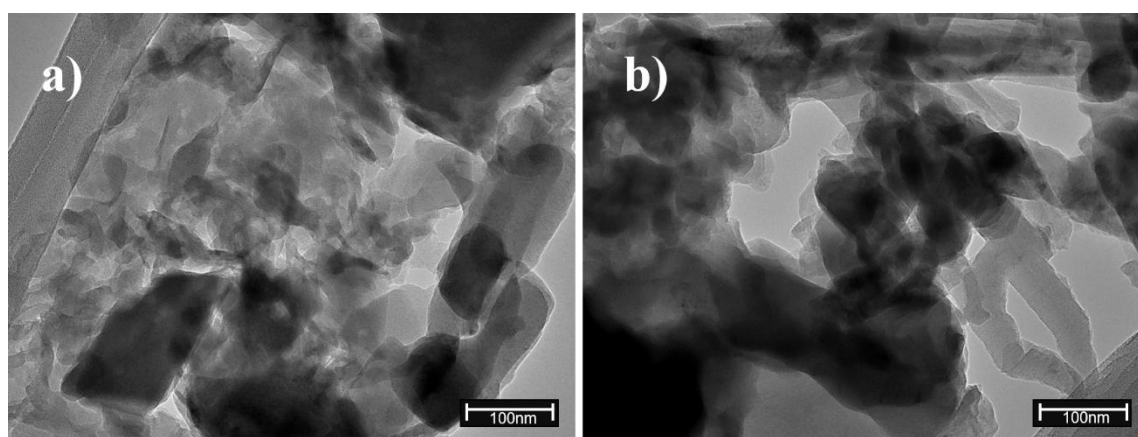

Figure 1 TEM image of a) CN and b) pCN

The ATR-FTIR spectra of CN and pCN are shown in Figure 3. The peak present at wavenumber 802 cm^{-1} represents the s-triazine ring unit [15].

While the peaks exist between 1200 cm^{-1} to 1650 cm^{-1} related to the C-N heterocycles skeleton stretching. Peaks on 1243, 1322, 1461, and 1623 cm^{-1}

derived from trigonal C-N(-C)-C (full condensation) and C-NH-C units (partial condensation) [16]. Then, peaks present between 3000 cm^{-1} to 3700 cm^{-1} (3104 cm^{-1}, 3278 cm^{-1}, 3411 cm^{-1}) were representing stretches of N-H and O-H due to the adsorbed of hydroxyl and free amino groups [17]. All of this characteristic peak present in both nanomaterials shown that pCN and CN were almost identical to each other.
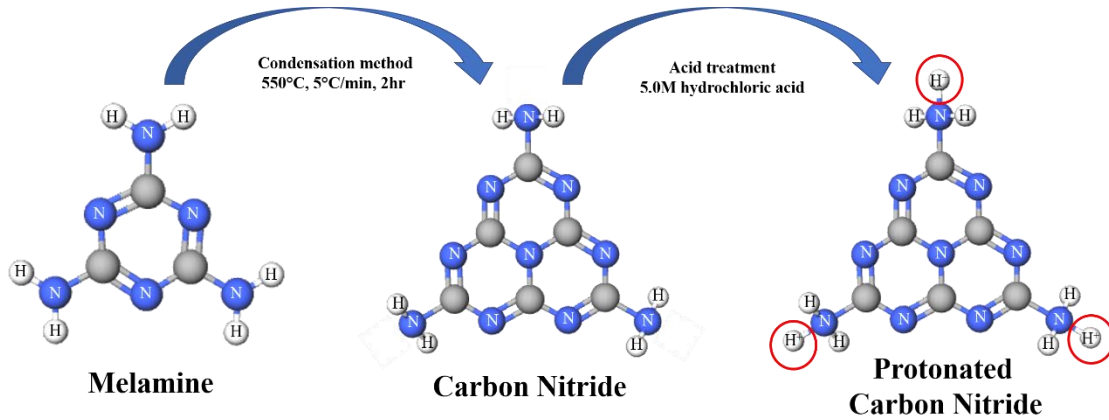
Figure 2 The schematic diagram that shows the formation of CN and pCN [14]
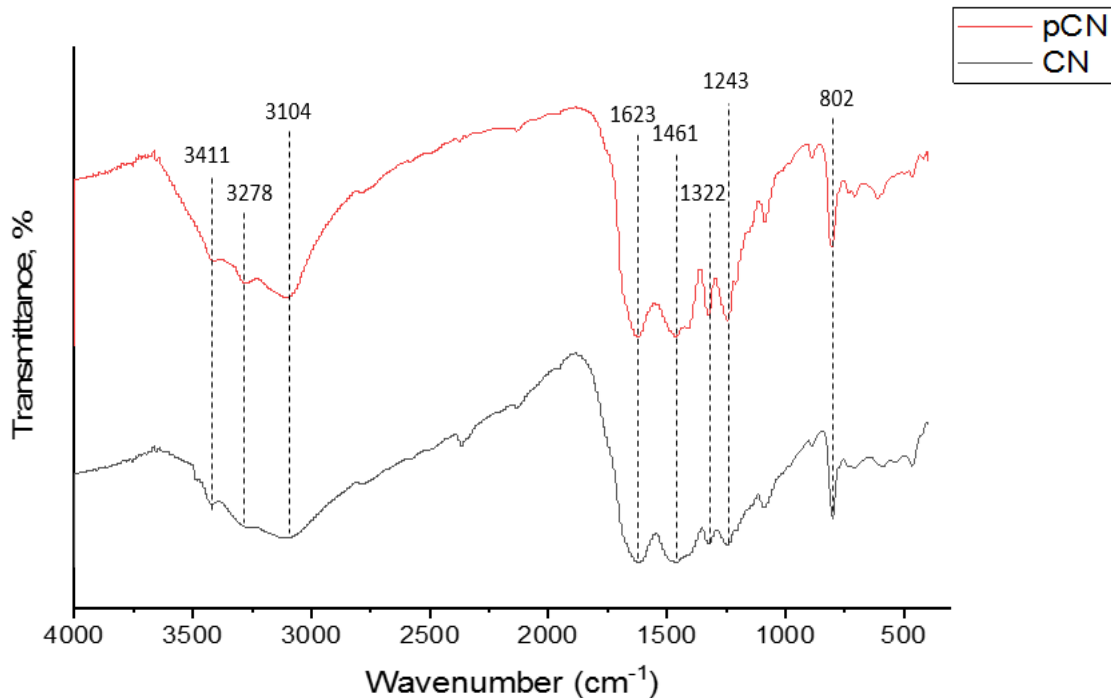
Figure 3 ATR-FTIR spectra of pCN and CN

Figure 4 presents the XRD patterns of CN and pCN. It can be seen that both of the nanomaterials still have 2 characteristic peaks even after being treated with acid. First peak that exist at 2-theta approximately 28.0º presenting the characteristic (002) interlayer-stacking distance (d-spacing) of CN that shown a graphene-like structure [18]. Upon protonation of CN, shifting of the peak was observed from 28.0° (d = 0.318nm) to 27.42° (d = 0.325nm). This means that d-spacing of planar graphitic structure of

CN was increased throughout the protonation process due to the existence of positive charge on the surface of the nanosheet [19, 20]. Another peak that present on approximately 12.48° was showing the structure of repeated s-triazine unit as shown in Figure 2. The same peak was observed by Niu *et al*. that fabricated CN through the same precursor with 4 hour durations [21]. By treating CN with strong acid like HCl, structure of repeated s-triazine was not affected [17].
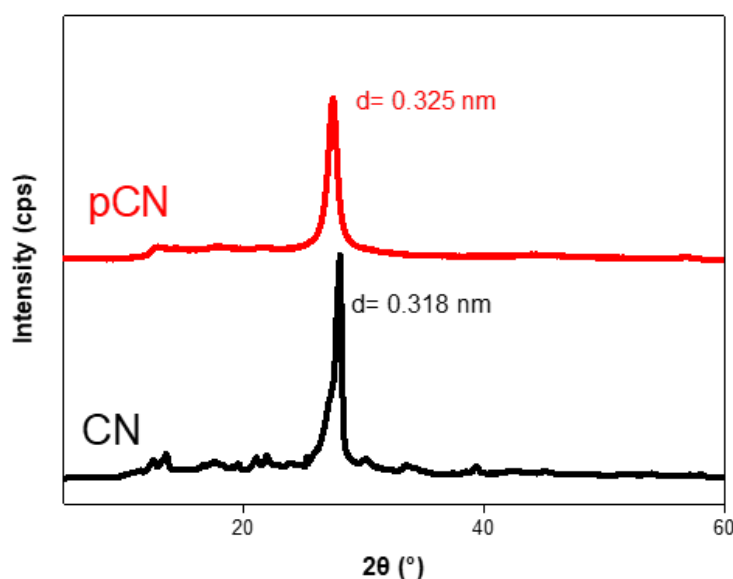

Figure 4 XRD pattern of CN and pCN

3.2 Characterization of Membrane

The membrane surface and cross-sectional morphology is illustrated in Figure 5. Figure 5A and 5B show the surface of PA layer on top of the PSf support membrane. Both of this membrane surface was showing a typical 'leaf-like' outgrowths and 'ridge-and-valley' structure that can be observed in any membrane with coating of a thin PA layer [22]. No noticeable difference in the morphology was observed since the membranes were not embedded with any

nanoparticles. The difference can be figure out on Figure 5C, 5D and 5E. Spot of the pCN nanoparticle can be seen and aggregation of nanoparticles were spotted when 0.15% loading of pCN was used in the PA layer. The cross-sectional images of TFC and TFN membrane prepared that consist of PA thin film layer and PSf substrate are shown in Figure 5 (a-e). From the cross-sectional images of the membrane, finger-like structure was observed. This type of structure were also observed by others work that applied the same dope formulation [23–25].
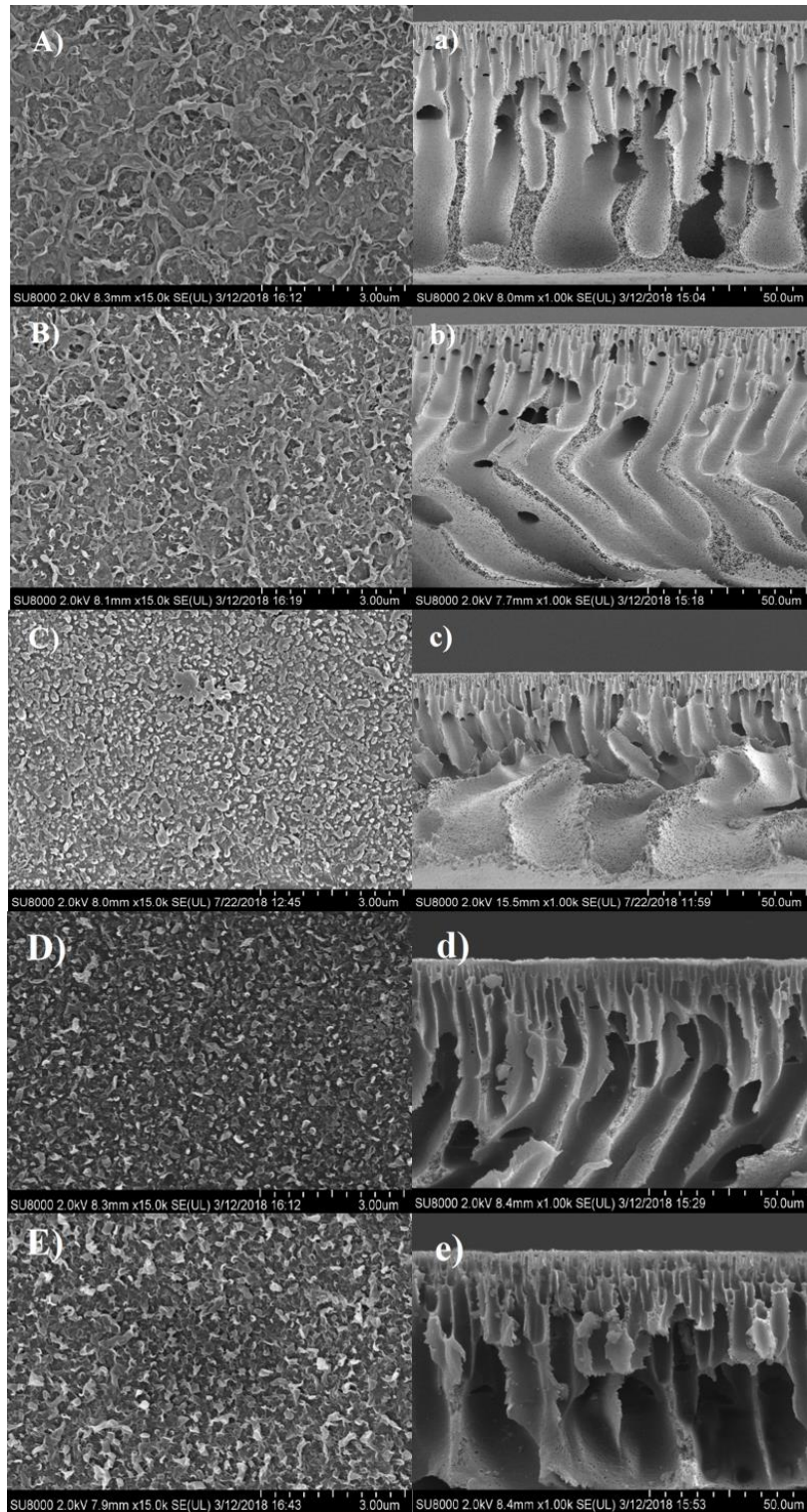
Figure 5 Surface (A-E) and cross section (a-e) FESEM image of TFC, pCN-TFN, 0.05 pCN-pCN-TFN, 0.1 pCN-pCN-TFN, and 0.15 pCN-pCN-TFN, respectively

Due to the low loading of pCN used in the PSf support membrane, cross sectional images did not show visible pCN nanoparticles. However, the existence of pCN in the substrate was evidenced with EDX elemental analysis as shown in Figure 6. It can be seen that pCN embedment increased the carbon and nitrogen composition because of it is the main element.
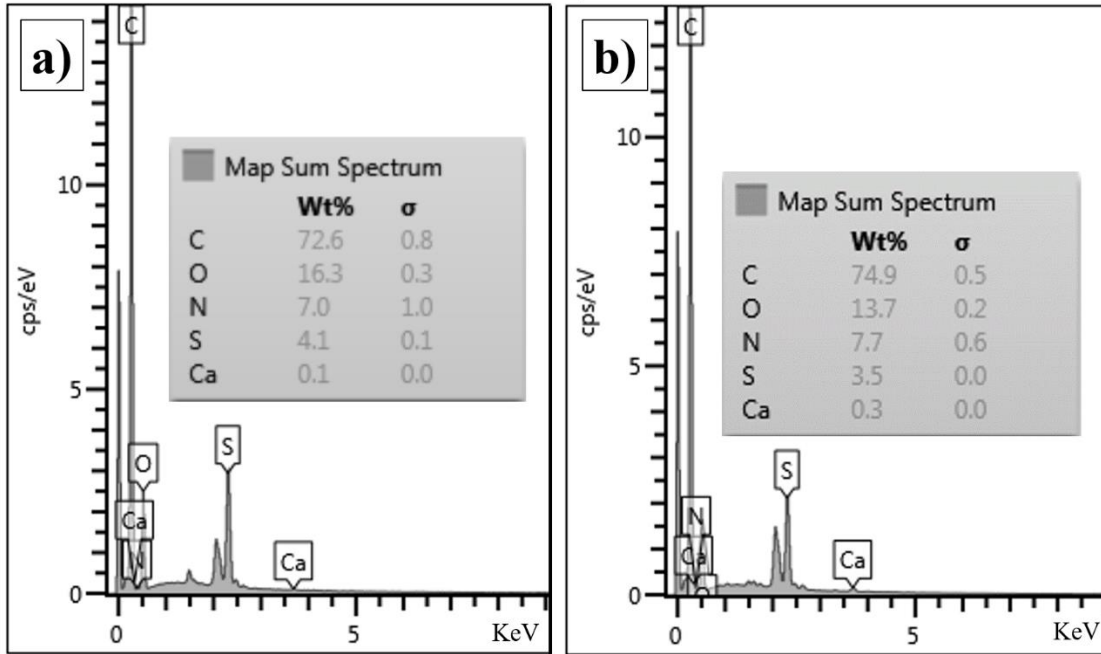
**Figure 6** EDX elemental analysis (a) TFC and (b) pCN-TFN

Figure 7 shows three-dimensional AFM images of the membranes with their average value of surface roughness (Ra). Surface roughness of the TFN membrane was influenced by PA layer that showed a ridge-and-valley structure which caused by the polymerized film of amine and acyl chloride monomers [8,26]. Figure 7a shows Ra = 34.71 nm for typical TFC membrane. While, the pCN-TFN membrane showed 35.37 nm for surface roughness since the embedded pCN within PSf support would increase the surface area [27]. This trend was also observed by Lai *et al*. [28] who used various loadings of graphene oxide (GO) to increase the surface roughness of the membrane. With embedding pCN on PA layer, the surface roughness is increase with increasing loading of pCN. Figure 7c showed the surface roughness increases to 36.35 nm when 0.05% of pCN were embedded on PA layer. This surface roughness values rapidly increase when higher loading of pCN were used to embedded pCN inside of the PA layer. Membrane 0.1 pCN-pCN-TFN (Figure 7d) and 0.15 pCN-pCN-TFN (Figure 7e) was showing 41.9 nm and 42.03 nm, respectively.

Table 2 recorded the contact angle and surface charge value of the prepared membranes. The contact angle measurement was used to determine the surface wettability of the membranes. The contact angles of TFC showed the highest value among the prepared membranes. TFC showed the contact

angle value of 88.92° ± 3.24 and decrease to 76.11° ± 3.33 after embedded of pCN inside the substrate. This due to the higher surface area produces when it has high surface roughness (shown in Figure 7). The same observation has been made by M. Rezaei-DashtArzhandi *et al.* [29] who used various loadings of CN. They reported that the contact angle decreased with increasing loading of nanoparticles. The surface charge was analysed by using zeta potential. TFC membranes exhibited surface charge value of -47.3mV. The pCN-TFN surface charge value was slightly increased to -35.7mV. This increase might be caused by the positive charge that carried by pCN in the substrate. This increment was observed when loadings of pCN were embedded in the PA layer. Surface charge for the membrane 0.05 pCN-pCN-TFN, 0.1 pCN-pCN-TFN and 0.15 pCN-pCN-TFN were showed about -28.2, -18.6 and -5.76, respectively. This negative charge surface on the membrane surface was needed to expel negative ion such as (Cl) hence preventing the ions from pass through the membrane [30].
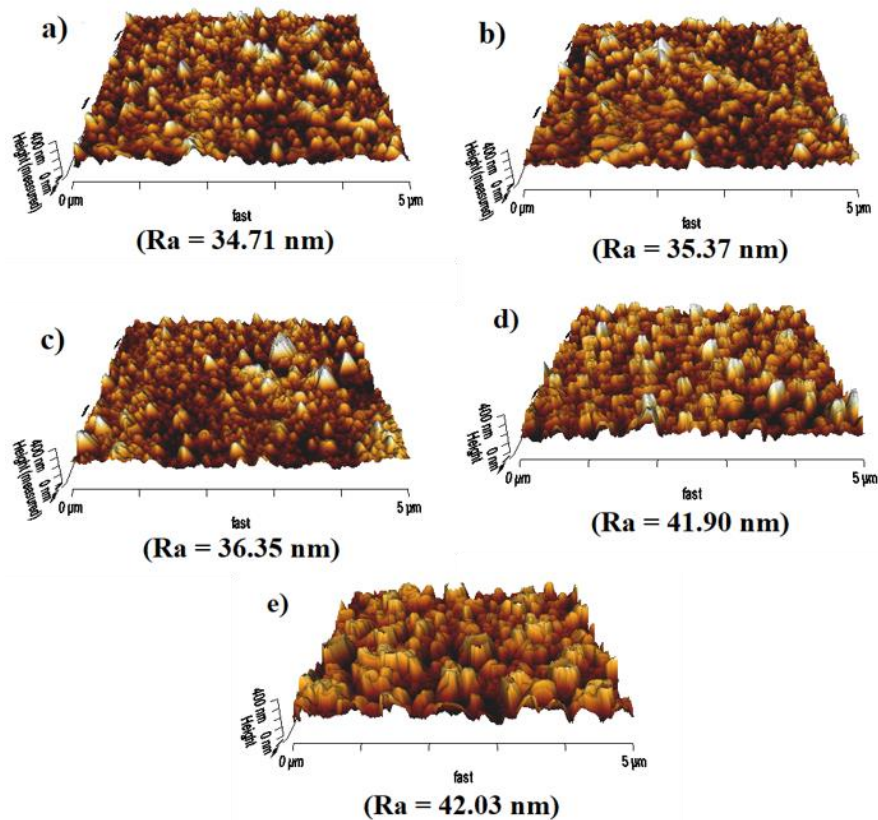
Figure 7 AFM images of (a) TFC, (b) pCN-TFN (c) 0.05 pCN-pCN-TFN, (d) 0.1 pCN-pCN-TFN, and (e) 0.15 pCN-pCN-TFN

Table 2 Surface charge and contact angle of TFC and TFN membrane

Membrane types	Contact angle (°)	Surface charge (mV)
TFC	88.92 ± 3.24	-47.3
pCN-TFN	76.11 ± 3.33	-35.7
0.05 pCN-pCN-TFN	59.74 ± 3.19	-28.2
0.1 pCN-pCN-TFN	57.39 ± 2.42	-18.6
0.15 pCN-pCN-TFN	52.61 ± 2.67	-5.76
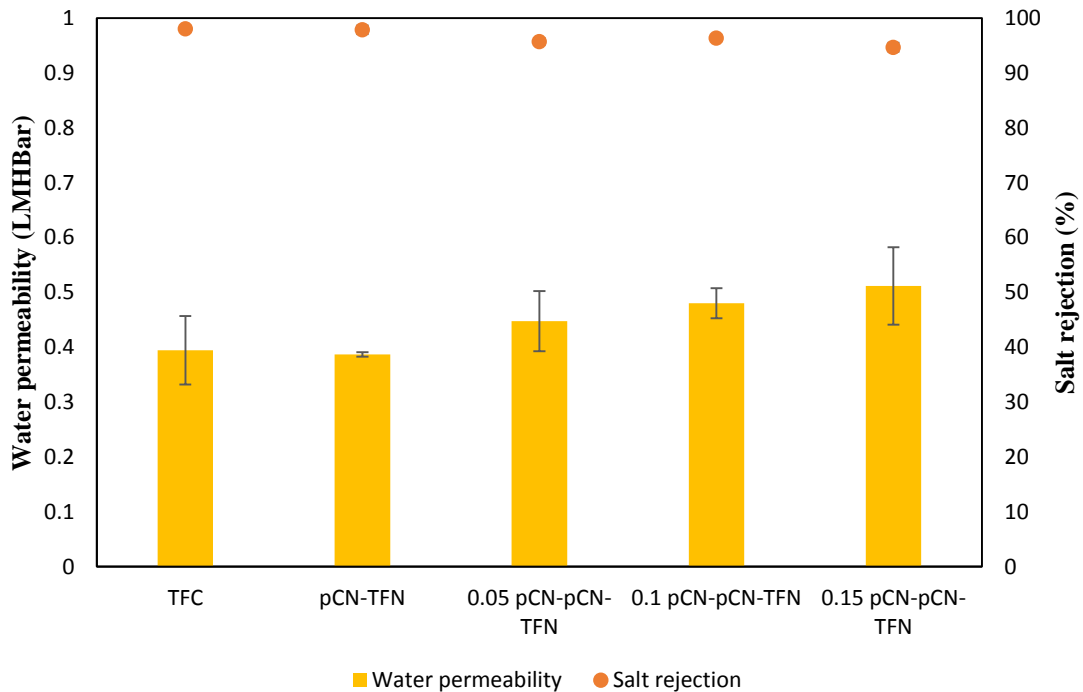
Figure 8 Water permeability and salt rejection of TFC and TFN membranes (test condition: 15 bar, 25°C, 2000ppm NaCl solution)

3.3 RO Performance

Water permeability and salt rejection performances of the membrane were illustrated in Figure 7. Based on the figure, the result of TFC and pCN-TFN membrane showed no significant different that can be measure. TFC membrane shows 0.39 LMHbar of water permeability with 98.0% NaCl rejection while pCN-TFN shows 0.38 LMHbar and 97.9%, respectively. The water permeability of the membrane was increased when loadings of pCN were embedded in the PA layer. The highest water permeability achieved was 0.15 pCN-pCN-TFN membrane with 0.51 LMHbar. Even though the water permeability was increased with higher loading of pCN, the salt rejection was compromised. The result shown that 0.15 pCN-pCN-TFN membrane has sacrifice

the salt rejection and dropped to 94.7%. This could happen due to the agglomeration of the nanoparticle thus affecting the formation of PA layer on top of the PSf support membrane. This trend has also been reported by Ma *et al.* [31] who used up to 0.2% loading of zeolite as nanofiller in the PA layer. They observed the decrement of salt rejection although the water permeability was increased.

4.0 CONCLUSION

In this work, pCN was obtained from the acid treatment of CN to alter its surface charge from negative to positive. The intention of embedding pCN within the PSf substrate was to increase the interaction between the PSf substrate and the PA layer where the PA layer can be strongly attached on the active layer of the substrate. Besides that, the desired properties of pCN in terms of high hydrophilicity have also positively affected the overall properties of the TFN. The samples prepared in this work, i.e. 0.05 pCN-pCN-TFN, 0.1 pCN-pCN-TFN and 0.15 pCN-pCN-TFN could significantly maintain the salt rejection while improving the water permeability. As a conclusion, this work gives an insight into the potential of applying pCN in modifying the structure and physico-chemical properties of the resultant TFN membranes, hence improving the desalination performance.

ACKNOWLEDGEMENT

REFERENCES

[1]   D. Pimentel, M. Burgess. 2015. World Human Population Problems. *Reference Module in Earth Systems and Environmental Sciences.* Elsevier Inc. 4: 313-317.

[2]   WWAP (United Nations World Water Assessment Programme). 2015. The United Nations World Water Development Report 2015: Water for a Sustainable World. Paris, UNESCO.

[3]   D. E. W. S. Loeb, S. Sourirajan. 1964. High Flow Porous Membranes for Separating Water from Saline Solutions.

[4]   V. Vatanpour, M. Safarpour, A. Khataee, H. Zarrabi. 2017. A Thin Film Nanocomposite Reverse Osmosis Membrane Containing Amine-functionalized Carbon Nanotubes. *Separation and Purification Technology.* 184: 135-143.

[5]   D. Emadzadeh, W. J. Lau, M. Rahbari-sisakht, A. Daneshfar, M. Ghanbari, A. Mayahi. 2015. A Novel Thin Film Nanocomposite Reverse Osmosis Membrane with Superior Anti-organic Fouling Affinity for Water Desalination. *DES.* 368: 106-113.

[6]   J. Farahbaksh, M. Delnavaz, V. Vatanpour. 2017. Investigation of Raw and Oxidized Multiwalled Carbon Nanotubes in Fabrication of Reverse Osmosis Polyamide Membranes for Improvement in Desalination and Antifouling Properties. *Desalination.* 410: 1-9.

[7]   Y. Wang, R. Ou, H. Wang, T. Xu. 2015. Graphene Oxide Modified Graphitic Carbon Nitride as a Modifier for Thin Film Composite Forward Osmosis Membrane. *J.*

Membr. Sci. 475: 281-289.

[8] I. W. Azelee, P. S. Goh, W. J. Lau, A. F. Ismail, K. C. Wong, M. N. Subramaniam. 2017. Enhanced Desalination of Polyamide Thin Film Nanocomposite Incorporated with Acid Treated Multiwalled Carbon Nanotube-titania Nanotube Hybrid. *Desalination.* 409: 163-170.

[9] S. C. Yan, Z. S. Li, Z. G. Zou. 2009. Photodegradation Performance of g-C3N4 Fabricated by Directly Heating Melamine. *Langmuir.* 25: 10397-10401

[10] M. Sihor, P. Praus, L. Svoboda, M. Ritz, I. Troppov, K. Ko. 2017. Graphitic Carbon Nitride: Synthesis, Characterization and Photocatalytic Decomposition of Nitrous Oxide, *Materials Chemistry and Physics.* 193: 438-446.

[11] J. Zhu, P. Xiao, H. Li, A. C. Carabineiro. 2014. Graphitic Carbon Nitride: Synthesis, Properties, and Applications in Catalysis. *Applied Materials and Interfaces.* 6: 16449-16465.

[12] I. A. Mudunkotuwa, V. H. Grassian, 2010. Citric Acid Adsorption on TiO2 Nanoparticles in Aqueous Suspensions at Acidic and Circumneutral Ph: Surface Coverage, Surface Speciation, and Its Impact on Nanoparticle - Nanoparticle Interactions. *J. Am. Chem. Soc.* 132: 14986-14994.

[13] B. W. Ninham. 1999. On Progress in Forces Since the DLVO Theory, *Advances in Colloid and Interface Science.* 83: 1-17.

[14] W. Ong, L. Tan, S. Chai, S. Yong, A. Rahman. 2015. Surface Charge Modification via Protonation of Graphitic Carbon Nitride (g-C3N4) for Electrostatic Self-assembly Construction of 2D / 2D Reduced Graphene Oxide (rGO)/g-C3N4 Nanostructures Toward Enhanced Photocatalytic Reduction of Carbon Dioxide to Metha. *Nano Energy.* 13: 757-770.

[15] L. Ma, H. Fan, K. Fu, S. Lei, Q. Hu, H. Huang, G. He. 2017. Protonation of Graphitic Carbon Nitride (g-C3N4) for Electrostatically Self-assembling Carbon @ g-C3N4 Core-shell Nanostructure Toward High Hydrogen Evolution. *Sustainable Chemistry and Engineering.* 5: 7093-7103.

[16] X. Zhang, J. Hu, H. Jiang. 2014. Facile Modification of a Graphitic Carbon Nitride Catalyst to Improve Its Photoreactivity Under Visible Light Irradiation. *Chemical Engineering Journal.* 256: 230-237.

[17] W. Ong, L. Tan, S. Chai, S. Yong, A. Rahman. 2015. Surface Charge Modification via Protonation of Graphitic Carbon Nitride (g-C3N4) for Electrostatic Self-assembly Construction of 2D / 2D Reduced Graphene Oxide (rGO)/ g-C3N4 Nanostructures toward Enhanced Photocatalytic Reduction of Carbon Dio. *Nano Energy.* 13: 757-770.

[18] Y. Zhang, A. Thomas, M. Antonietti, X. Wang. 2009. Activation of Carbon Nitride Solids by Protonation : Morphology Changes. Enhanced Ionic Conductivity, and Photoconduction Experiments. *J. Am. Chem. Soc.* 4: 50-51.

[19] C. Huang, W. Zhang, Z. Yan, J. Gao, W. Liu, P. Tong, L. Zhang. 2015. Protonated Mesoporous Graphitic Carbon Nitride for Rapid and Highly Efficient Removal of

Microcystins. *RSC Adv.* 5: 45368-45375.

[20] J. Wang, D. Hao, J. Ye, N. Umezawa. 2017. Determination of Crystal Structure of Graphitic Carbon Nitride: Ab Initio Evolutionary Search and Experimental Validation. *Chemistry of Material*s. 29: 2694-2707.

[21] R. Niu, L. Kong, L. Zheng, H. Wang, H. Shi. 2017. Novel graphitic Carbon Nitride Nanosheets/sulfonated Poly (ether ether ketone) Acid-base Hybrid Membrane for Vanadium Redox Flow Battery. *Journal of Membrane Science.* 525: 220-228.

[22] G. N. B. Baroña, J. Lim, M. Choi, B. Jung. 2013. Interfacial Polymerization of Polyamide-aluminosilicate SWNT Nanocomposite Membranes for Reverse Osmosis. DES. 325: 138-147.

[23] X. Zhang, J. Tian, Z. Ren, W. Shi, Z. Zhang. 2016. High performance Thin-film Composite (TFC) Forward Osmosis (FO) Membrane Fabricated on Novel Hydrophilic Disulfonated Poly (Arylene Ether Sulfone) Multiblock Copolymer/Polysulfone Substrate. *Journal of Membrane Science*. 520: 529-539.

[24] T. Sirinupong, W. Youravong, D. Tirawat, W. J. Lau, G. S. Lai, A. F. Ismail. 2017. Synthesis and Characterization of Thin Film Composite Membranes Made of PSF-TiO2/GO Nanocomposite Substrate for Forward Osmosis Applications. *Arabian Journal of Chemistry.* 11: 1144-1153.

[25] D. Emadzadeh, W. J. Lau, A. F. Ismail. 2013. Synthesis of Thin Film Nanocomposite Forward Osmosis Membrane with Enhancement in Water Flux without Sacrificing Salt Rejection. *DES.* 330: 90-99.

[26] B. Khorshidi, T. Thundat, D. Pernitsky, M. Sadrzadeh. 2017. Permeation Properties of Thin Film Composite Polyamide Membrane. *Journal of Membrane Science.* 535: 248-257.

[27] B. Jeong, E. M. V Hoek, Y. Yan, A. Subramani, X. Huang, G. Hurwitz, A. K. Ghosh, A. Jawor. 2007. Interfacial Polymerization of Thin Film Nanocomposites : A New Concept for Reverse Osmosis Membranes. *J. Memb. Sci.* 294: 1-7.

[28] G. S. Lai, W. J. Lau, P. S. Goh, A. F. Ismail, N. Yusof, Y. H. Tan. 2016. Graphene Oxide Incorporated Thin Film Nanocomposite Nanofiltration Membrane for Enhanced Salt Removal Performance. *DES.* 387: 14-24.

[29] M. Rezaei-dashtarzhandi, M. H. Sarrafzadeh, P. S. Goh, W. J. Lau, A. F. Ismail. 2018. Development of Novel Thin Film Nanocomposite Forward Osmosis Membranes Containing Halloysite/Graphitic Carbon Nitride Nanoparticles Towards Enhanced Desalination Performance. *DES.* 447: 18-28.

[30] M. R. Teixeira, M. J. Rosa, M. Nyström. 2005. The Role of Membrane Charge on Nanofiltration Performance. *Journal of Membrane Science*. 265: 160-166.

[31] N. Ma, J. Wei, R. Liao, C. Y. Tang, 2012. Zeolite-polyamide Thin Film Nanocomposite Membranes : Towards Enhanced Performance

for Forward Osmosis. *Journal of Membrane Science.* 405-406: 149-157.